Information Fusion 103 (2024) 102106

Contents lists available at ScienceDirect

Information Fusion

journal homepage: www.elsevier.com/locate/inffus

Software defined radio frequency sensing framework for Internet of Medical Things

Najah AbuAli [a,*], Mohammad Bilal Khan [a,b], Farman Ullah [a], Mohammad Hayajneh [a], Hikmat Ullah [a], Shahid Mumtaz [c]

[a] College of Information Technology, United Arab Emirates University, P.O. Box 15551, Al Ain, Abu Dhabi, United Arab Emirates
[b] Department of Electrical and Computer Engineering, COMSATS University Islamabad, Attock Campus, Kamra Road, Attock, 43600, Punjab, Pakistan
[c] Nottingham Trent University, 50 Shakespeare Street, Nottingham, NG14FQ, UK

ARTICLE INFO

Keywords:
Deep learning
IoMT
Respiratory abnormalities
RF sensing
SDR

ABSTRACT

The escalating demand for biomedical systems that can precisely diagnose and manage critical diseases underscores the need for innovative solutions. A non-invasive and intelligent Internet of Medical Things (IoMT) system emerges as a promising technology, potentially enabling physicians to assess patients with reduced health risks. The respiratory rate is a pivotal vital sign among the primary clinical assessments. The allure of Radio Frequency (RF) sensing lies in its ability to monitor respiratory patterns without direct contact. However, the practical implementation of such systems often necessitates supplementary hardware to manage the extensive data and radio functionalities, leading to concerns related to cost and feasibility. Software-Defined Radio (SDR) technology presents itself as a viable solution to these challenges. This research introduces a comprehensive framework for the IoMT system, aiming to diagnose respiratory abnormalities early through RF sensing and SDR technology. We employ a deep learning framework and compare its performance with traditional machine learning models to ensure reliable and precise classification of respiratory abnormalities. The achieved results underscore the superiority of deep learning frameworks over conventional machine learning models in classifying respiratory anomalies. Specifically, the deep learning framework exhibits exceptional performance in discerning the temporal dependencies and patterns inherent in respiratory abnormalities, achieving an average accuracy exceeding 98% for each respiratory abnormality classification.

1. Introduction

Within the vast expanse of Internet of Things (IoT) applications, the Internet of Medical Things (IoMT) emerges as a particularly transformative force in healthcare [1,2]. By integrating sensors, devices, and data analytics, the IoMT promises to revolutionize patient care, streamline healthcare operations, and elevate the overall quality of medical services. Central to the success of IoMT is its capability for information fusion, which amalgamates data from diverse sources to ensure comprehensive, real-time patient monitoring [3,4]. This fusion of information is not just a technological advancement; it represents a paradigm shift in how healthcare can be delivered, monitored, and optimized. Respiratory health, a critical part of overall well-being, offers a window into the broader implications of such advancements. Alterations in respiratory patterns can be indicative of a wide range of health issues, from mild conditions like allergies to severe disorders such as asthma, COPD, lung cancer, and sleep apnea, which is characterized by intermittent cessation of breathing during sleep [5,6]. Environmental exposure to smoke, pollution, and allergens can also lead to abnormal respiratory patterns. Early detection and monitoring of these patterns are crucial not only for effective treatment but also for enhancing the quality of life for affected individuals. Existing technologies, including pulse oximeters, spirometers, and peak flow meters, have undeniably advanced the field [7–9]. However, they come with inherent challenges. Issues related to accuracy, patient discomfort due to invasive methods, limited mobility due to tethered devices, and the constraints of remote monitoring are some of the pressing concerns that the current landscape faces [10]. Addressing these challenges requires a novel approach that combines cutting-edge technology with the unique requirements of respiratory health monitoring. In this research, we present such an approach by integrating software-defined radio (SDR) technology with RF sensing within the IoMT framework. This integration is not merely a technological amalgamation, but represents

* Corresponding author.
E-mail address: najah@uaeu.ac.ae (N. AbuAli).

https://doi.org/10.1016/j.inffus.2023.102106
Received 15 June 2023; Received in revised form 7 October 2023; Accepted 30 October 2023
Available online 7 November 2023

a paradigm shift in the way respiratory health can be monitored. By offering a contactless, precise, and intelligent monitoring system, we aim to overcome the limitations of existing technologies. The employment of deep learning techniques further accentuates the system's diagnostic capabilities, offering a distinctive, data-driven perspective in the field of respiratory health monitoring [11,12]. Our contributions to this field are multifaceted.

- At the forefront is the proposed innovative IoMT framework, which harnesses the power of RF sensing and SDR technology to provide early and contactless diagnosis of respiratory abnormalities, including sleep apnea. This system is designed with the patient's comfort in mind, eliminating the need for invasive sensors or tethered devices.
- To ensure the accuracy and reliability of the data, we employ advanced signal-processing algorithms. These algorithms refine the raw data, eliminating noise and artifacts thereby enhancing the accuracy of respiratory rate measurements.
- The proposed approach is the implementation of a deep learning framework, specifically designed for classifying respiratory patterns. In comparative analyses, this framework consistently outperforms conventional machine learning models, highlighting its effectiveness and potential to revolutionize respiratory health monitoring.

The proposed research explores the combination of IoMT, SDR technology, and deep learning, and its potential to transform healthcare [13,14]. By addressing gaps in the current literature and introducing a flexible, scalable, and efficient framework, we aim to establish a new benchmark for IoMT-based healthcare solutions, with a focus on respiratory health. This synergy has the potential to improve patient outcomes and contribute to the advancement of the healthcare industry.

The paper is organized into five sections. Section 2 discusses the available techniques for the intelligent diagnosis of health disorders using SDR technology and RF sensing, and deep learning for building a platform. In Section 3, the methods and materials are presented to develop an intelligent and contactless diagnosis of respiratory abnormalities. Section 4 involves the analysis of the results and a discussion on the performance evaluation of the classification accuracy of respiratory abnormalities using deep learning and machine learning models. Finally, Section 5 concludes the paper and presents future recommendations for the developed system, along with suggestions to improve it in the future.

2. Related work

The significance of diagnosing respiratory abnormalities is paramount, given the prevalence and potential severity of associated conditions. Extensive research has been dedicated to using RF signals and SDR technology for the intelligent classification of health disorders. In [15], an SDR-based system was introduced for human activity recognition (HAR). This system, marked by its flexibility and scalability, showcased the potential of SDR technology in sensing human health disorders. Furthermore, [16] demonstrated the detection of hand movements using RF sensing and SDR technology, while [17] expanded the scope to detect both small-scale movements (such as breathing and coughing) and large-scale movements (hand movements).

The versatility of SDR technology was further highlighted by [18], which introduced a contactless through-the-walls (TTW) smart sensing system to monitor human physical activity during isolation. Their approach, which utilized fine-grained wireless channel state information data, achieved a classification accuracy of 99.7% for various physical activities using machine learning models. However, such advances were not limited to activity recognition. In [19], postures were detected after spinal cord surgery, achieving a classification accuracy of 99.6%.

Although these studies undeniably advanced the field, a recurring theme was the focus on binary classification problems, often distinguishing between 'normal'and 'abnormal'states [20]. Such an approach, although effective in controlled environments, may not be robust enough for real-world applications with multifaceted data.

The potential of SDR technology in respiratory health was explored by [21], which achieved a classification accuracy of 99.4% for abnormal respiratory patterns. Similarly, [22] introduced a system that could detect Cheyne-Stokes respiration in patients with heart failure, achieving a diagnostic accuracy of 97%. A significant challenge of the RF detection system is the accurate monitoring of multiple persons in the same environment. While [23] presented a system that could achieve a classification accuracy of 99.7% for a single person, the accuracy dropped to 93.5% and 88.4% for two and three persons, respectively. This decline in accuracy underscores the complexities introduced when multiple individuals are present in the same environment. Factors such as overlapping RF signals, interference, and unique respiratory patterns of each individual can confound the system, making accurate detection and classification more challenging. Despite these advances, a significant limitation persisted: manual design of complex features to train machine learning models [24]. This not only made model comparisons challenging due to the lack of standard datasets but also raised concerns about the applicability of these models to large, real-world datasets.

Deep learning, with its ability to automatically extract features, has recently emerged as a promising solution to these challenges. While Convolutional Neural Networks (CNNs) have been widely adopted for image-based medical diagnoses [25–29], their efficacy in time-series data remains debated [30]. On the other hand, recurring neural networks (RNNs) have shown promise in learning sequential and temporal features, as evidenced by their applications in natural language processing (NLP), audio, and speech processing [31,32]. Hybrid models, combining CNNs and RNNs, have also been explored, especially for video data classification, demonstrating success in learning both spatial and temporal features [33].

Recent studies have also explored deep learning for biomedical diagnosis based on audio data. For example, [34] used a chest mounted sensor to collect audio data from human speech and coughing, which was then classified using a CNN-RNN hybrid model. Similarly, [35,36] employed deep learning models to classify sleep apnea disorders and heart sounds, respectively. In [37], proposes an innovative solution that uses long short-term memory (LSTM) networks to differentiate between apnea and hypopnea episodes. The research demonstrates the model's effectiveness in classifying episodes and estimating the respiratory event index. This offers a promising alternative to traditional diagnostic methods. The deep learning model's performance is significant and has shown valuable contributions to medical applications.

In summary, while significant advances have been made in the domain of RF signal-based sensing and SDR technology for the classification of health disorders, gaps persist. The prevalent focus on binary classification and the manual feature crafting in machine learning models highlight the need for more robust, automated solutions. Our research, as delineated in the introduction, aims to bridge these gaps, offering our contribution by integrating IoMT, SDR technology, and deep learning for a comprehensive solution to respiratory health monitoring.

3. Materials and methods

The IoMT framework uses RF sensing and SDR technology to detect and classify respiratory abnormalities through four processing units: respiration abnormalities time series data collection, signal processing, classification, and internet gateway.

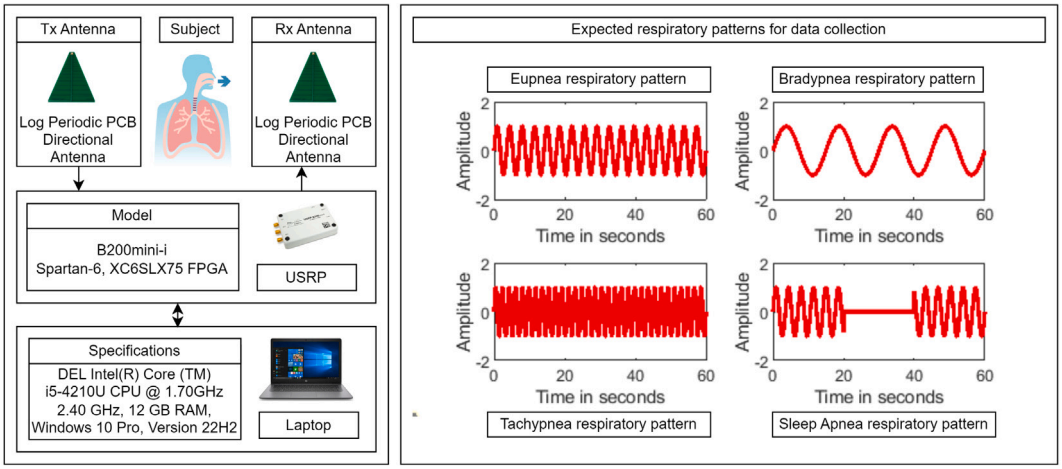

Fig. 1. Data collection using SDR technology-based RF sensing.

3.1. Data collection

The RF sensing platform, leveraging SDR technology, facilitates non-invasive data acquisition pertaining to respiratory anomalies, as depicted in Fig. 1. This platform combines a universal software radio peripheral device (USRP), a computer laptop, and a pair of directional antennas. The USRP device is responsible for delineating radio functionalities, which are orchestrated via a proprietary code developed within the LabVIEW software environment housed on the laptop. Parameters such as operating frequency, sampling rate, and antenna gain are meticulously defined within this software. Directional antennas play a pivotal role in both the transmission and reception of electromagnetic (EM) waves, thus evaluating the wireless channel state information (WCSI) at the receiving end. WCSI provides invaluable information on the wireless channel. The presence of a human within this channel invariably results in a distinctive channel frequency response (CFR) due to macro-movements like hand and leg motions, and micro-movements such as those of the chest and abdomen. For the purposes of this research, the focus is predominantly on micro-movements associated with respiratory anomalies, all of which are meticulously extracted within a controlled laboratory setting.

The study encompasses data from four distinct respiratory patterns: Eupnea (standard relaxed breathing), Bradypnea (decelerated breathing rate), Tachypnea (accelerated breathing rate), and Sleep Apnea (a sleep disorder characterized by intermittent cessation of breathing). The data set is enriched by incorporating subjects from diverse demographics of age. Before data acquisition, each participant undergoes a comprehensive orientation through a video demonstration. It is imperative to note that the data acquisition platform has no adverse implications on human health. All experimental procedures are initiated after securing both verbal and written consent from the participants. A detailed description of the real-time experimental setup for data acquisition is available in Fig. 2. The complete details of the data acquisition are tabulated in Table 1.

3.2. Data prepossessing

Data preprocessing is a pivotal phase in extracting subjective information from the data set. Raw data obtained from the RF sensing platform are loaded with extraneous channel information, which can obscure the desired trends of respiratory abnormalities, potentially leading to erroneous diagnostic information. Hence, rigorous data preprocessing is indispensable for extracting salient information from the dataset. This study employs a comprehensive preprocessing regimen that includes cleaning, selection of subcarriers, smoothing, and normalization, as shown in Fig. 3.

Table 1
Data collection information on respiratory abnormalities.

Sr. No	Information	Quantity/Operating
1	USRP Devices	1
2	Antennas	2
3	Frequency in GHz	4.8
4	Distance between Antennas in Feets	4
5	Height of the Antennas in Feets	1.5
6	Sampling Rate (S/s)	200
7	Samples	12 000
8	Laptops	1
9	Subjects	25
10	Total Experiments	100
11	Total subcarriers	256
12	Selected subcarriers	146
13	Activity duration in seconds	60
14	Number of activities	4
15	Each activity records	3650
16	Total number of records	14 600

3.2.1. Denoising

Denoising is executed using the discrete wavelet transform (DWT). The data received from the RF sensing system are often marred by high-level impulses and extraneous signal bursts. Conventional denoising methodologies, such as low-pass filters (LPF) and median filters (MF), exhibit suboptimal performance for intricate applications [38]. While, in theory, an LPF or MF should effectively filter out these superfluous signals, residual noise often persists, thereby altering the signal's intrinsic information. Thus, direct application of these filters for denoising is inadvisable. Advanced filtering paradigms, especially those based on wavelet transform, are adept at meticulously filtering out undesired signals from RF sensing data, particularly given their prowess in discerning human respiratory patterns. When configured with optimal wavelet transform parameters, these filters effectively eliminate residual noise, yielding a lucid respiratory pattern, thereby surpassing conventional denoising techniques. The wavelet transform (WT) has garnered significant attention in signal processing, with numerous researchers leveraging it to discern valuable frequency information [39].

3.2.2. Sub-carrier selection

The orthogonal frequency division multiplexing (OFDM) is used to accurately extract granular information during transmission and reception. 256 sub-carriers are concurrently received from each CFR. As illustrated in Fig. 3, the amplitude variations of different sub-carriers exhibit differential sensitivities to respiratory behaviors attributable to their distinct sub-carrier frequencies. Notably, nulls and DC sub-carriers

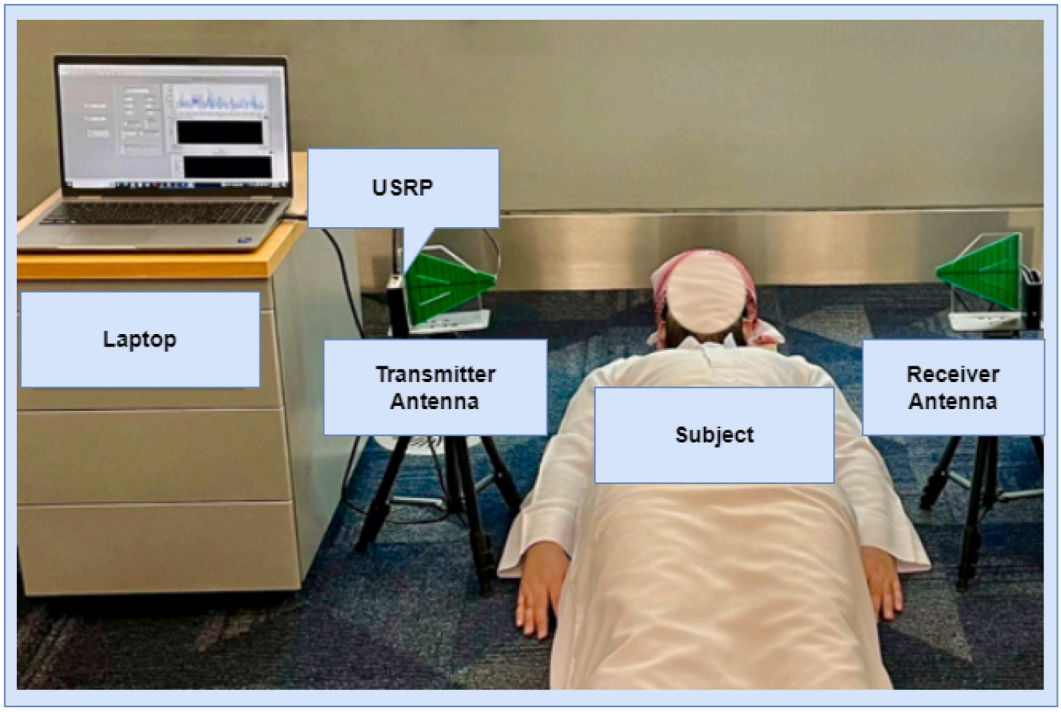

Fig. 2. Real-time experimental setup.

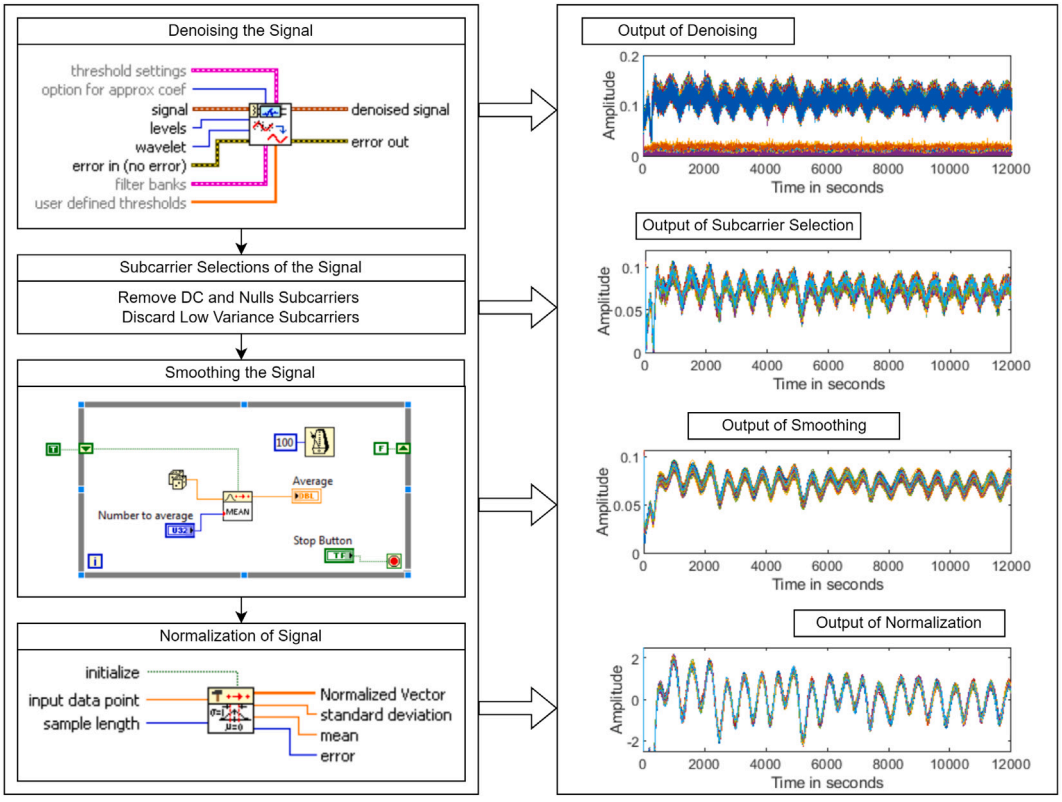

Fig. 3. Signal processing of primary data.

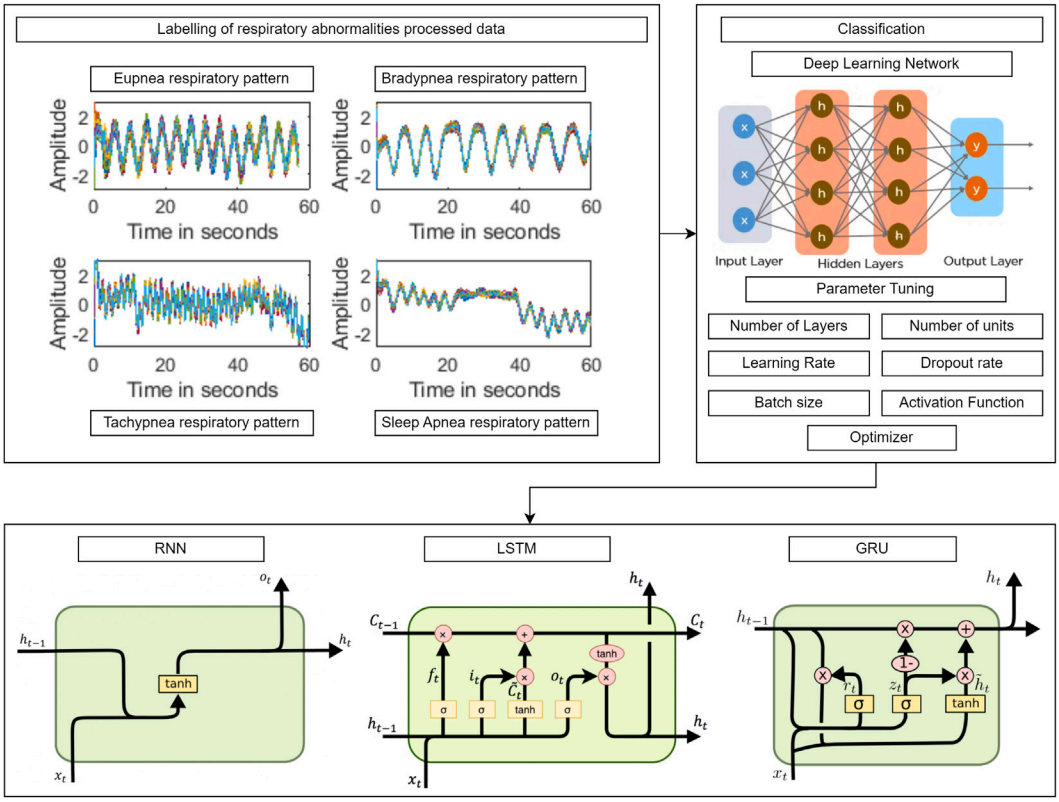

Fig. 4. Classification of using deep learning models.

manifest minimal amplitude variations, rendering them unsuitable for respiratory data analysis, necessitating their exclusion from the dataset. Sub-carriers with diminished sensitivity can also impede accurate respiration detection and are thus prudently 110 subcarriers were removed. This study adopts the higher-variance scoring method to select subcarriers, given their heightened sensitivity to human respiration.

3.2.3. Smoothing

For signal refinement, a moving average filter is deployed. This finite impulse response filter is instrumental in mitigating short-term surges or random noise perturbations, ensuring the preservation of the right respiratory pattern. A linear moving average is applied, with a window size of 256, to the input time series data to enhance the clarity of respiratory patterns.

3.2.4. Normalization

The refined respiratory patterns undergo normalization using the statistical profile (μ, σ_s) of the time series data, where μ and σ_s denote the mean and standard deviation, respectively. The objective is to achieve a normalized respiratory pattern with a statistical profile of $(0, 1)$. Here, Y represents the output time series data of the normalized respiratory pattern, X represents the input respiratory pattern of length x, and x_i is the ith sample of X. Normalization is pivotal for enhancing the efficacy of certain AI models, especially those reliant on distance-based metrics or specific data distributions. By judiciously scaling the features, the algorithm can more precisely discern inter-variable relationships, culminating in better classification outcomes.

3.3. Classification

For the classification of time series data of respiratory abnormalities using a deep learning framework, the initial step involves labeling the data of the processed time series of respiratory patterns with the corresponding breathing abnormality, as illustrated in Fig. 4.

Table 2
Deep learning models parameters tuning.

Sr.No	Parameter	Tunning
1	Numbers of Layers	1
2	Numbers of Hidden Units	16, 32, 64
3	Learning Rate	0.2
4	Dropout Rate	0.2
5	Batch size	32, 64, 128
6	Dense Layer Activation Function	Softmax
7	Epochs	50
8	Optimizer	Adam

This study evaluates the performance of both deep and conventional machine learning models in terms of classification accuracy for the respiratory abnormalities dataset. The deep learning frameworks under scrutiny include recurrent neural networks (RNN), long-short-term memory (LSTM), bidirectional LSTM (Bi-LSTM), gated recurrent units (GRU), and bidirectional GRU (Bi-GRU). The hyperparameter optimization process is carried out to improve model performance, with the specific tuning parameters defined in Table 2.

3.3.1. RNN model

The Recurrent Neural Network (RNN) is a neural architecture adept at processing sequential data by leveraging historical inputs and their associated outputs. Its inherent feedback connections facilitate the retention of prior inputs, enhancing its predictive capabilities for subsequent data points. Given its proficiency in discerning temporal dependencies, the RNN model is particularly suited for time series data. For time series data for respiratory abnormalities, the RNN model assimilates antecedent respiratory patterns to categorize the present respiratory pattern. Recurrent linkage in the RNN model ensures seamless information transition from one temporal step to the next within the dataset.

Unlike conventional neural networks, the forward and backward propagation processes of the RNN model are distinct due to their recurrent nature. At each temporal step t, the RNN model receives an input vector x_t, representing the current sample in the respiratory pattern time series. This input, in conjunction with the preceding hidden state h_{t-1}, undergoes a series of weight multiplications to compute h_t. The resultant hidden state h_t is contingent on the RNN architecture, as articulated in Eq. (1).

$$h_t = \sigma_h\left(U_h \times x_t + V_h \times h_{t-1} + b_h\right) \tag{1}$$

In Eq. (1), matrices U_h and V_h represent weights, b_h signifies the bias vector, and σ_h denotes the activation function applied on a per-sample basis. Subsequently, the hidden state h_t is utilized to compute the output o_t for the current temporal step, as delineated in Eq. (2):

$$o_t = \sigma_o\left(W_o \times h_t + b_o\right) \tag{2}$$

Eq. (2) specifies that W_o represents the weight matrix, b_o is the bias vector, and σ_o is the sample-wise applied activation function. This procedure is reiterated for each sample in the time series data, with each iteration updating h_t and generating an o_t for each t. Subsequently, a loss function is formulated by evaluating the predicted o_t with the target o_t for that specific t. Depending on the task at hand, various loss functions, such as the mean squared error (MSE) for classification, can be employed. Gradients of this loss, relative to the RNN model's parameters (weights and biases), are then computed. This computation is executed independently for each t, factoring in all antecedent t contributions. The chain rule facilitates gradient calculation. These gradients are then harnessed to refine the RNN model's weight matrix and bias vector via the Adam optimizer. The overarching objective is to minimize the cumulative loss across all temporal steps. During backpropagation, gradients for each t are aggregated and retroactively propagated to update the RNN model's weight matrices and bias vectors. It is imperative to note that traditional RNNs are susceptible to the vanishing gradient problem (VGP). This implies that during extensive backpropagation through numerous temporal steps, gradients can either attenuate or amplify. Advanced RNN variants like LSTM and GRU were conceptualized to circumvent this limitation, which integrate specialized gating mechanisms to capture long-standing dependencies adeptly [40].

3.3.2. LSTM model

The Long Short-Term Memory (LSTM) model is an evolved RNN architecture methodically crafted to counteract the VGP and adeptly capture enduring dependencies in sequential data. By introducing intricate gating mechanisms and memory cells, the LSTM model orchestrates the flow of information within the network. Analogous to other RNN architectures, at each temporal step t, the input x_t is channeled into the LSTM model, representing the current sample in the time series. Central to the LSTM model is a memory cell, tasked with preserving and updating information temporally. The preceding cell state, C_{t-1}, combined with the current x_t, yields a new candidate cell state $\widetilde{C}_t$, as expressed in Eq. (3).

$$\widetilde{C}_t = tanh\left(W_c \times x_t + U_c \times C_{t-1} + b_c\right) \tag{3}$$

Eq. (3) elucidates that W_c and U_c are weight matrices, b_c is the bias vector, and the activation is typically the hyperbolic tangent ($tanh$) function. The forget gate, a pivotal component, arbitrates the retention or discarding of information from C_{t-1}. By processing the x_t and h_{t-1} through a sigmoid activation, a forget gate vector f_t is derived, as detailed in Eq. (4).

$$f_t = \sigma\left(W_f \times x_t + U_f \times h_{t-1} + b_f\right) \tag{4}$$

Eq. (4) specifies that W_f and U_f are weight matrices, and b_f is the bias vector, with σ being the sigmoid activation function. The input gate discerns the new information to be stored in C_t. By processing the x_t and h_{t-1} through a sigmoid activation, an input gate vector i_t is derived, as articulated in Eq. (5).

$$i_t = \sigma\left(W_i \times x_t + U_i \times h_{t-1} + b_i\right) \tag{5}$$

Eq. (5) clarifies that W_i and U_i are weight matrices, and b_i is the bias vector, specific to i_t and $\widetilde{C}_t$ candidate update vector. The output o_t ascertains which segments of C_t should be relayed as h_t. By processing the x_t and h_{t-1} through a sigmoid activation, an output o_t is derived, as depicted in Eq. (6).

$$o_t = \sigma\left(W_o \times x_t + U_o \times h_{t-1} + b_o\right) \tag{6}$$

Eq. (6) explicates that W_o and U_o are weight matrices, and b_o is the bias vector, specific to o_t. Refreshed C_t is derived by combining f_t, i_t, and o_t, as illustrated in Eq. (7).

$$C_t = f_t \times C_{t-1} + i_t \times g_t \tag{7}$$

The hidden state h_t is deduced by multiplying the output gate with the updated C_t, post the application of the $tanh$ activation function, as presented in Eq. (8).

$$h_t = o_t \times tanh(C_t) \tag{8}$$

The resultant h_t can be harnessed for diverse applications, such as prognostications or generating subsequent samples in the time series. A loss function is formulated by evaluating the predicted output or h_t in each t with the target output or h_t. Gradients of this loss, relative to the LSTM's parameters (weights and biases), are then computed. This intricate process entails gradient computation for each t independently and considering all subsequent t contributions. These gradients are retroactively propagated, factoring in the recurrent connections and the gating mechanisms intrinsic to the LSTM architecture. The gradients for each temporal step are aggregated and backpropagated to refine the LSTM's weights and biases. The LSTM's gating mechanisms ensure that gradients traverse temporally without vanishing or exploding. The gates f_t, i_t, and o_t modulate information and gradient flow, empowering the LSTM to discern and retain enduring dependencies in time series data.

3.3.3. Bi-LSTM model

The Bidirectional LSTM (Bi-LSTM) is an enhancement of the LSTM architecture, designed to assimilate information from both the antecedent and subsequent temporal steps. This dual-layer architecture comprises two LSTM layers: one processing the time series data in a forward trajectory and the other in a reverse trajectory. At each temporal step t, the Bi-LSTM receives an input x_t, emblematic of the current sample in the time series. This input is concurrently channeled into both the forward and reverse LSTM layers. The forward LSTM layer processes the input from the beginning to the conclusion of the time series, while the reverse LSTM layer operates in the opposite direction. At each temporal step, the forward and reverse hidden states, hf_t and hb_t, are combined to form a unified hidden state. This combined state can be employed for diverse tasks, such as predictions or generating subsequent samples in the time series. A loss function is formulated by evaluating the predicted output or h_t in each t with the target output or h_t. Gradients of this loss, relative to the Bi-LSTM's parameters (weights and biases), are then computed. This intricate process entails gradient computation for each t independently, while also considering contributions from both forward and reverse trajectories. These gradients are retroactively propagated, factoring in recurrent connections in both the forward and reverse LSTM layers. The gradients for each temporal step are aggregated and back-propagated to refine the Bi-LSTM's weights and biases. By combining gradients from both trajectories at each temporal step, the Bi-LSTM ensures bidirectional information flow, enhancing the learning process. This bidirectional approach empowers the Bi-LSTM to discern dependencies from both antecedent and subsequent contexts, making it crucial for tasks necessitating a holistic comprehension of the input time series data.

3.3.4. GRU model

The Gated Recurrent Unit (GRU) is a refined variant of RNN created to counteract VGP and capture enduring dependencies in sequential data. By merging the forget and input gates into a single update gate, the GRU streamlines the LSTM architecture. At each temporal step t, the GRU receives an input x_t, representative of the current sample in the time series. This input is channeled into the GRU network, where the update gate arbitrates the retention of h_{t-1} and the incorporation of new information. This gate processes x_t and h_{t-1} through a sigmoid activation, resulting in an update gate vector z_t, as shown in Eq. (9).

$$z_t = \sigma\left(W_z \times x_t + U_z \times h_{t-1} + b_z\right) \tag{9}$$

Eq. (9) clarifies that W_z and U_z are weight matrices, and b_z is the bias vector. The reset gate, another pivotal component, determines which segments of h_{t-1} should be discarded. By processing the x_t and h_{t-1} through a sigmoid activation, a reset gate vector r_t is derived, as detailed in Eq. (10).

$$r_t = \sigma\left(W_r \times x_t + U_r \times h_{t-1} + b_r\right) \tag{10}$$

Eq. (10) specifies that W_r and U_r are weight matrices, and b_r is the bias vector. The reset gate r_t is then used to calculate a candidate hidden state $\widetilde{h}_t$, which represents the new information to be incorporated into h_t. This computation, which processes the x_t and h_{t-1} through the hyperbolic tangent activation function $tanh$, yields $\widetilde{h}_t$, as presented in Eq. (11).

$$\widetilde{h}_t = tanh\left(W(r_t \times h_{t-1}) + U \times x_t + b\right) \tag{11}$$

Eq. (11) explicates that W and U are weight matrices, and b is the bias vector. The hidden state h_t is refreshed by integrating h_{t-1} and $\widetilde{h}_t$ using the update gate z_t, as illustrated in Eq. (12).

$$h_t = \left(1 - z_t \times h_{t-1} + z_t \times \widetilde{h}_t\right) \tag{12}$$

A loss function is formulated by computing the predicted output or h_t at each t with the target output or h_t. Gradients of this loss, relative to the GRU's parameters (weights and biases), are then computed. This elaborate process involves the calculation of the gradient for each t independently, while also considering all subsequent t contributions. These gradients are retroactively propagated, incorporating the recurrent connections essential to the GRU architecture. The gradients for each temporal step are aggregated and back-propagated to refine the GRU's weights and biases. During this backpropagation, the update and reset gates modulate the gradient flow, enabling the GRU to discern which segments of the hidden state to retain or refresh. The update gate modulates the information transition from the antecedent hidden state to the current one, while the reset gate arbitrates which segments of the antecedent hidden state to discard. Consequently, the GRU captures enduring dependencies while maintaining a more streamlined architecture than its LSTM counterpart.

3.3.5. Bi-GRU model

The Bidirectional GRU (Bi-GRU) is an enhancement of the GRU architecture, designed to assimilate information from both antecedent and subsequent temporal steps. This dual-layered architecture comprises two GRU layers: one processing the time series data in a forward trajectory and the other in a reverse trajectory. At each temporal step t, the Bi-GRU receives an input x_t, representative of the current sample in the time series. This input is concurrently channeled into both the forward and reverse GRU layers. The forward GRU layer processes the input from the beginning to the conclusion of the time series, while the reverse GRU layer operates in the opposite direction. At each temporal step, the forward and reverse hidden states are combined to form a unified hidden state. This combined state can be employed for diverse tasks, such as predicting or generating subsequent samples in the time series. A loss function is formulated by evaluating the predicted output or h_t in each t with the target output or h_t. Gradients of this loss, relative to the Bi-GRU's parameters (weights and biases), are then computed. This intricate process entails gradient computation for each t independently, while also considering contributions from both forward and reverse trajectories. These gradients are retroactively propagated, factoring in recurrent connections in both the forward and reverse GRU layers. The gradients for each temporal step are aggregated and back-propagated to refine the Bi-GRU's weights and biases. By combining gradients from both trajectories at each temporal step, the Bi-GRU ensures bidirectional information flow, enhancing the learning process. This bidirectional approach empowers the Bi-GRU to discern dependencies from both antecedent and subsequent contexts, making it crucial for tasks necessitating a holistic comprehension of the input time series data.

These deep learning architectures are used to classify time series data related to respiratory abnormalities. By discerning temporal dependencies and identifying indicative patterns, they can detect anomalies. The choice of a specific model is contingent upon the data's characteristics and the problem's distinctions, with parameter tuning further optimizing performance.

3.4. Internet gateway

The gateway, fortified with a deep learning model for the classification of respiratory abnormalities, harnesses RF detection based on the SDR technology dataset, as shown in Fig. 5, collects classified respiratory abnormality data, and performs preliminary processing tasks. Given the confidential nature of medical data, the gateway is presumed to be stimulated with robust security protocols. Furthermore, it adheres to stringent healthcare data regulations, such as the Health Insurance Portability and Accountability Act (HIPAA) or the General Data Protection Regulation (GDPR) [41].

4. Results and discussion

This section presents the results of the analysis of the respiratory abnormalities time series dataset using both deep learning and traditional machine learning algorithms. The dataset, which encompasses four distinct breathing patterns, was subjected to classification to identify four types of respiratory abnormalities. A comparative assessment was conducted to evaluate the performance of deep learning models against their machine learning counterparts. For this comparative study, the machine learning models employed include Ensemble Bagged Trees (EBT), Quadratic Support Vector Machine (QSVM), Fine K Nearest Neighbor (FKNN), Fine Tree (FT), and Kernel Naïve Bayes (KNB). The evaluation methodology incorporated a five-fold cross-validation (5-CV) technique.

Convergence curves, accuracies, and confusion matrices are employed to provide a granular understanding of the classification results. The accuracy and loss convergence curves for deep learning models are evaluated by varying the epochs, batch sizes, and hidden units. In Fig. 6, the accuracy and loss convergence of both the training and validation curves are presented for deep learning models. Initially, accuracy is not very high, but with the increasing number of epochs, the accuracy is improved for all the deep learning models. The loss convergence curves are also improved for both the training and validation by increasing the number of epochs. In Fig. 7, a performance comparison of the deep learning models using various batch sizes is presented. The results conclude that the accuracy of the deep learning models follows the trends by varying the batch size. Fig. 8 depicts the performance comparison of deep learning models using various hidden units. The results conclude that increasing the hidden units increases the accuracy of the deep learning models and this trend is almost present in all the deep learning models used in this research. So, we use the 64 hidden units for all deep learning for the rest of our implementation.

Table 3 presents the confusion matrix for deep learning models applied to the time series data collected from the RF sensing system.

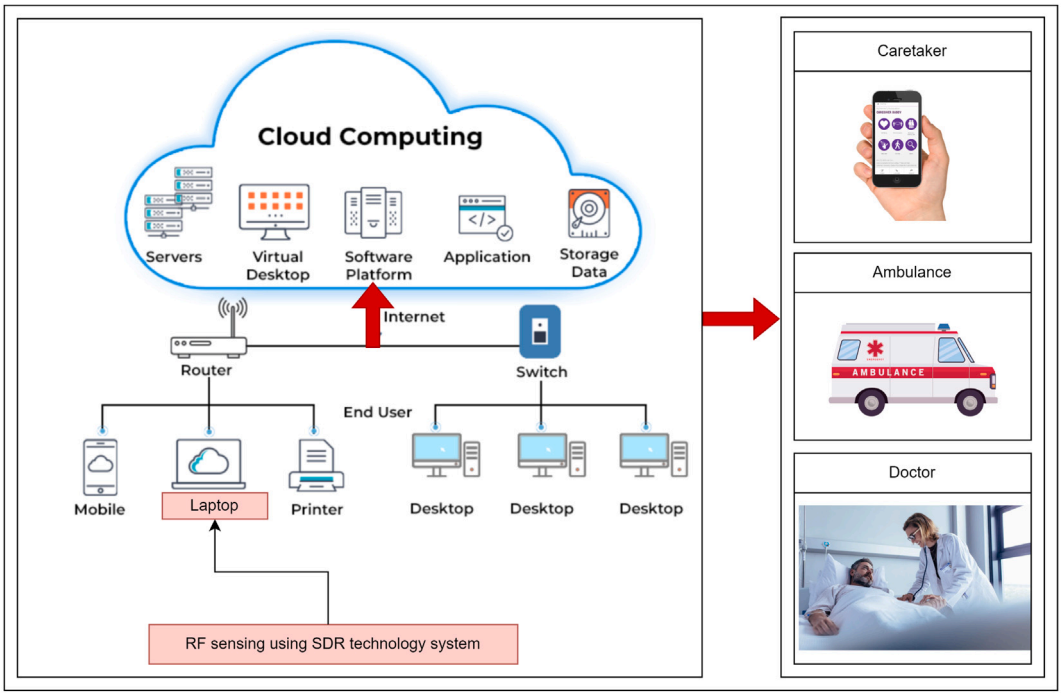

Fig. 5. Information communicated to healthcare services through Internet.

Table 3
Confusion matrix of respiratory abnormalities data using deep learning models.

Models	Actual/Predicted	Eupnea	Bradypnea	Tachypnea	Sleep Apnea
RNN	Eupnea	3645	0	1	4
	Bradypnea	18	3523	35	74
	Tachypnea	0	1	3647	2
	Sleep Apnea	13	48	20	3569
LSTM	Eupnea	3650	0	0	0
	Bradypnea	6	3593	7	44
	Tachypnea	0	0	3647	3
	Sleep Apnea	6	53	5	3586
Bi-LSTM	Eupnea	3649	0	0	1
	Bradypnea	7	3602	10	31
	Tachypnea	0	0	3649	1
	Sleep Apnea	1	52	7	3590
GRU	Eupnea	3648	1	0	1
	Bradypnea	4	3590	7	49
	Tachypnea	0	2	3647	1
	Sleep Apnea	8	47	9	3586
Bi-GRU	Eupnea	3649	1	0	0
	Bradypnea	4	3615	1	30
	Tachypnea	0	4	3645	1
	Sleep Apnea	2	43	10	3595

For instance, the RNN model accurately predicted 3645 Eupnea samples, while misclassifying 5. 3523 samples were correctly predicted as Bradypnea and 127 were misclassified. 3647 samples were correctly predicted as Tachypnea, and 3 were misclassified. 3569 samples were correctly predicted as Sleep Apnea, and 81 were misclassified. The LSTM, Bi-LSTM, GRU, and Bi-GRU models exhibited analogous patterns.

The LSTM model showed superior performance in predicting the Eupnea class, with all 3650 samples correctly predicted and without misclassifications. However, the model had 3 misclassifications out of 3650 samples predicted as Tachypnea and 81 misclassifications out of 3650 samples predicted as Sleep Apnea. For Bradypnea, the model had 3593 correct predictions and 57 misclassifications.

The Bi-LSTM model showed similar performance in predicting Eupnea, with 3649 correct predictions and only one misclassification. Similarly, only one sample was misclassified out of 3650 samples predicted as Tachypnea. However, the model had 60 misclassifications, and 3590 were correctly predicted as Sleep Apnea and 48 misclassifications out of 3650 samples for Bradypnea.

The GRU model correctly predicted 3648 samples as Eupnea, with only two misclassifications. However, the model had 60 misclassifications for Bradypnea and 64 misclassifications for Sleep Apnea, out of 3650 samples. For Tachypnea, the model had 3647 correct predictions and 3 misclassifications. The Bi-GRU model had similar performance in predicting Eupnea, with 3649 correct predictions and only one misclassification. However, the model had 55 misclassifications for Sleep Apnea and 35 misclassifications for Bradypnea, and 3595 and 3615 were correctly predicted, respectively. The model had 5 misclassifications out of 3650 samples predicted as Tachypnea.

Deep learning models generally showed high accuracy in predicting the Eupnea class, with very few misclassifications. However, the models had varying degrees of success in predicting the other classes (Bradypnea, Tachypnea, and Sleep Apnea), with some models having more false positives or false negatives than others. These results suggest that deep

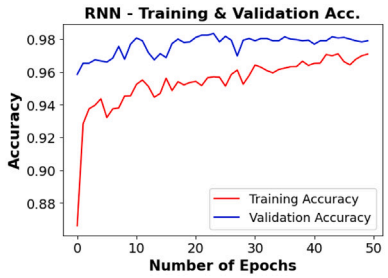

(a) Accuracy of the RNN model.

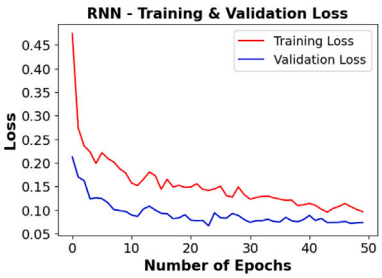

(b) Loss of the RNN model.

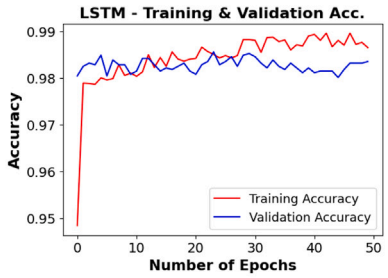

(c) Accuracy of the LSTM model.

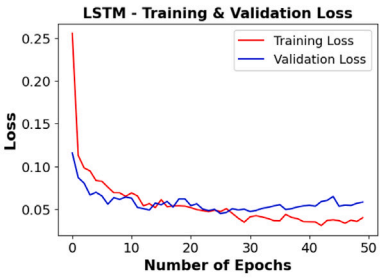

(d) Loss of the LSTM model.

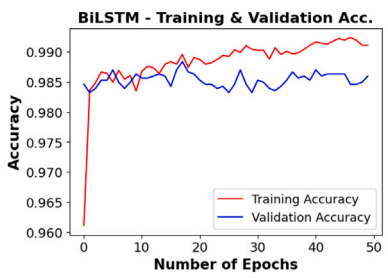

(e) Accuracy of the Bi-LSTM model.

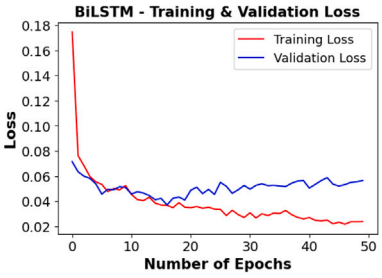

(f) Loss of the Bi-LSTM model.

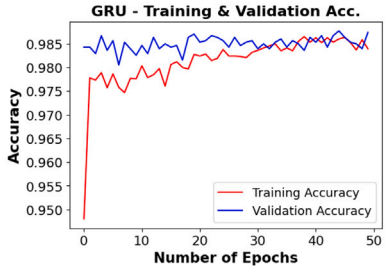

(g) Accuracy of the GRU model.

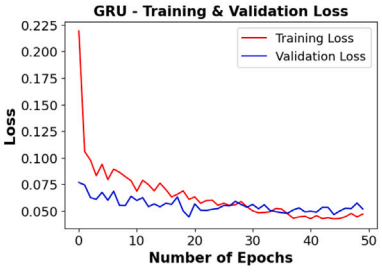

(h) Loss of the GRU model.

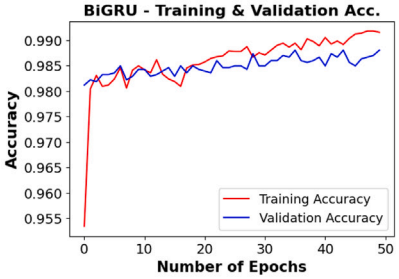

(i) Accuracy of the Bi-GRU model.

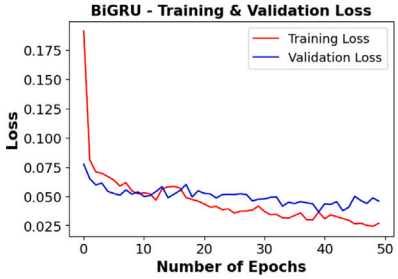

(j) Loss of the Bi-GRU model.

Fig. 6. Accuracy and loss curves for all the deep learning models.

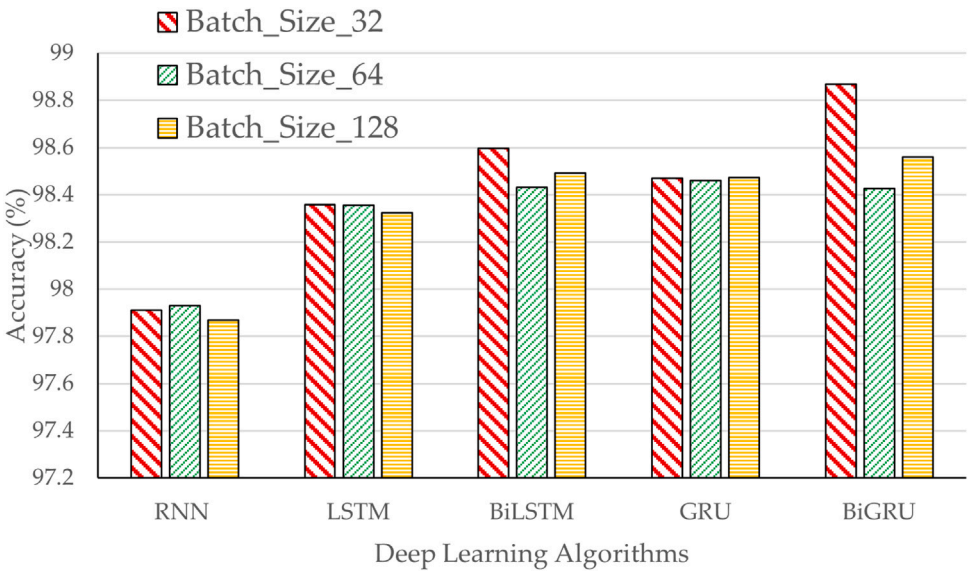

Fig. 7. Performance comparison of deep learning models using various batch sizes.

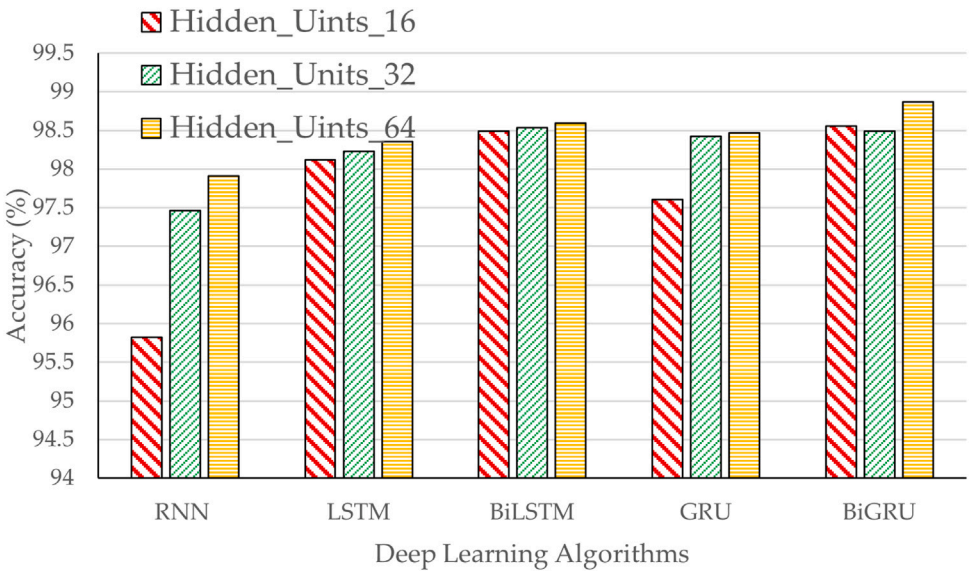

Fig. 8. Performance comparison of deep learning models using various hidden units.

learning models may be useful in predicting respiratory disorders, but further research is needed to improve their accuracy and effectiveness.

Table 4 presents the confusion matrix for several machine-learning models that were used to classify four respiratory patterns based on the collected time-series data from the RF sensing system. The EBT model correctly predicted 3476 samples as Eupnea, but 174 samples were misclassified. Similarly, 3462 samples were correctly predicted as Bradypnea, but there were 188 misclassified samples. The Tachypnea classification was correct for 3514 samples, but 136 samples were misclassified. Finally, the Sleep Apnea classification was correct for 3404 samples, but 246 were misclassified.

The Q-SVM model showed 3401 correct predictions for Eupnea, but there were 249 misclassified samples. For Bradypnea, 3470 samples were correctly classified, but there were 180 misclassified samples. The Tachypnea classification was correct for 3443 samples, but there were 207 misclassified samples. Finally, there were 3311 correct predictions for Sleep Apnea, but 339 were misclassified.

In the FK-NN model, 3332 samples were correctly predicted as Eupnea, but 318 samples were misclassified. Similarly, 3372 samples were correctly predicted as Bradypnea, but there were 278 misclassified samples. The Tachypnea classification was correct for 3416 samples, but 234 samples were misclassified. Finally, the Sleep Apnea classification was correct for 3336 samples, but 314 were misclassified.

The FT model showed 3076 correct predictions for Eupnea, but 574 samples were misclassified. For Bradypnea, 2919 samples were correctly predicted, but 731 samples were misclassified. There were 3066 correct predictions for Tachypnea, but 564 samples were misclassified. Finally, there were 2866 correct predictions for Sleep Apnea, but 784 were misclassified.

The KNB model showed that only 2443 samples were correctly predicted as Eupnea, while 1217 samples were misclassified. Similarly, 2501 samples were correctly predicted as Bradypnea, but 1149 samples were misclassified. There were 2141 correct predictions for Tachypnea, but 1509 samples were misclassified. Finally, there were 2391 correct predictions of Sleep Apnea, but 1259 samples were misclassified.

The EBT, Q-SVM, FK-NN, FT, and KNB models demonstrated varying degrees of classification accuracy. However, it is noteworthy that

Table 4
Confusion matrix of respiratory abnormalities data using machine learning models.

Models	Actual/Predicted	Eupnea	Bradypnea	Tachypnea	Sleep Apnea
EBT	Eupnea	3476	72	27	75
	Bradypnea	74	3462	21	93
	Tachypnea	69	9	3514	58
	Sleep Apnea	63	160	23	3404
Q-SVM	Eupnea	3401	72	48	129
	Bradypnea	71	3470	8	101
	Tachypnea	76	7	3443	124
	Sleep Apnea	151	139	49	3311
FK-NN	Eupnea	3332	120	96	102
	Bradypnea	86	3372	32	160
	Tachypnea	98	29	3416	107
	Sleep Apnea	93	129	92	3336
FT	Eupnea	3076	194	197	183
	Bradypnea	425	2919	140	166
	Tachypnea	217	104	3066	263
	Sleep Apnea	260	388	136	2866
KNB	Eupnea	2433	559	158	500
	Bradypnea	371	2501	230	548
	Tachypnea	582	300	2141	627
	Sleep Apnea	289	695	275	2391

Table 5
Performance analysis of machine and deep learning models.

Machine learning		Deep learning	
Model	Accuracy	Model	Accuracy
EBT	94.91%	RNN	98.52%
Q-SVM	93.32%	LSTM	99.16%
FK-NN	92.27%	Bi-LSTM	99.24%
FT	81.72%	GRU	99.21%
KNB	64.89%	Bi-GRU	99.34%

the KNB model exhibited a much higher misclassification rate as compared to all other machine learning models.

Table 5 offers an evaluation of the classification accuracies between deep learning and machine learning models. The findings underscore that deep learning models, including RNN, LSTM, Bi-LSTM, GRU, and Bi-GRU, outperform their machine learning counterparts in terms of accuracy, achieving metrics ranging between 98.18% and 98.52%. In contrast, the machine learning models' accuracy spanned between 64.89% and 94.91%.

The results derived from deep learning models underscore their robustness in the classification of respiratory abnormalities. These models consistently demonstrated high accuracy in various respiratory patterns, emphasizing their outperformance accuracy level. Such findings suggest that the intricate architectures of time series deep learning models, including RNN, LSTM, BiLSTM, GRU, and BiGRU, are more suitable for this classification task compared to conventional machine learning models. The higher classification accuracy of deep learning models can be attributed to their intrinsic ability to autonomously discern and extract salient features from the raw input data. These architectures possess the ability to internalize complex patterns and relationships within the data, facilitating more precise predictions. On the contrary, traditional machine learning models often require manual feature engineering, potentially constraining their ability to detect subtle variations in respiratory abnormalities.

In summation, the empirical findings of this study demonstrate the competence of deep learning models in the precise classification of respiratory abnormalities. These findings are of significant relevance to healthcare practitioners and researchers in the domain of the diagnosis and monitoring of respiratory ailments. Leveraging deep learning models can potentially enhance the accuracy and efficiency of respiratory abnormality detection, paving the way for enhanced patient care and timely interventions.

5. Conclusion

This paper introduced an intelligent, contactless SDRF sensing framework tailored for IoMT. Empirical evaluations underscored the framework's precision and reliability, positioning it as a valuable tool for contemporary healthcare services. Its potential to non-invasively diagnose respiratory ailments augments safety protocols, safeguarding medical professionals from direct patient contact. The system accurately classified four distinct respiratory patterns: Eupnea, Bradypnea, Tachypnea, and Sleep Apnea, leveraging advanced deep-learning models. Comprehensive evaluations revealed that the BiGRU deep learning model outperformed its counterparts, achieving a classification accuracy of 98.52%. Furthermore, a comparative analysis between deep learning and traditional machine learning models was conducted, highlighting the superior performance of the former in terms of classification accuracy. Such findings accentuate the merits of integrating deep learning algorithms within health diagnostic systems.

While the primary focus of this study was respiratory pattern classification, prospective research endeavors could broaden the system's diagnostic capabilities to encompass a myriad of health conditions. This expansion might necessitate the integration of multifaceted sensors or metrics to encapsulate a comprehensive spectrum of health indicators. It is imperative to rigorously evaluate the system's robustness and consistency across diverse scenarios and ambiances. Such evaluations could entail system trials on larger and more heterogeneous datasets, encompassing a diverse demographic and health spectrum. Further inquiries should also delve into the pragmatic implementation of this framework within real-time medical ecosystems, addressing potential challenges and ensuring its harmonious integration within existing healthcare infrastructures. By regarding these future recommendations, this research can catalyze the evolution and refinement of intelligent, non-intrusive health diagnostic frameworks, thereby fortifying the growing domain of IoMT.

CRediT authorship contribution statement

Najah AbuAli: Investigation, Conceptualization, Methodology, Writing – review & editing, Funding acquisition, Research administration. **Mohammad Bilal Khan:** Conceptualization, Methodology, Data curation, Writing – original draft. **Farman Ullah:** Software, Formal analysis, Validation, Writing – review & editing. **Mohammad Hayajneh:** Conceptualization, Validation, Writing – review & editing. **Hikmat Ullah:** Data curation, Software. **Shahid Mumtaz:** Writing – review & editing.

Declaration of competing interest

The authors declare that they have no known competing financial interests or personal relationships that could have appeared to influence the work reported in this paper.

Data availability

Data will be made available on request.

Acknowledgments

This work was supported by Zayed Health Center at UAE University under Fund code G00003476.

References

[1] F. Alshehri, G. Muhammad, A comprehensive survey of the Internet of Things (IoT) and AI-based smart healthcare, IEEE Access 9 (2020) 3660–3678.
[2] J. Ali, R.H. Jhaveri, M. Alswailim, B.-h. Roh, ESCALB: An effective slave controller allocation-based load balancing scheme for multi-domain SDN-enabled-IoT networks, J. King Saud Univ.-Comput. Inf. Sci. 35 (6) (2023) 101566.
[3] Y. Cheng, K. Wang, H. Xu, T. Li, Q. Jin, D. Cui, Recent developments in sensors for wearable device applications, Anal. Bioanal. Chem. 413 (24) (2021) 6037–6057.
[4] A. Awad, M.M. Fouda, M.M. Khashaba, E.R. Mohamed, K.M. Hosny, Utilization of mobile edge computing on the Internet of Medical Things: A survey, ICT Express (2022).
[5] C.K. Grissom, B.E. Jones, Respiratory health benefits and risks of living at moderate altitude, High Altitude Med. Biol. 19 (2) (2018) 109–115.
[6] A.V. Devereaux, H. Backer, A. Salami, C. Wright, K. Christensen, K. Rice, C. Jakel-Smith, M. Metzner, J.K. Bains, K. Staats, et al., Oxygen and ventilator logistics during California's COVID-19 surge: when oxygen becomes a scarce resource, Disaster Med. Public Health Preparedness 17 (2023) e33.
[7] A.M. Luks, E.R. Swenson, Pulse oximetry for monitoring patients with COVID-19 at home. Potential pitfalls and practical guidance, Ann. Am. Thoracic Soc. 17 (9) (2020) 1040–1046.
[8] B. Theja, K. Shobha, C. Keshavamurthy, H. Chandrashekar, Spirometry, 2023.
[9] A. Anisa, T. Hamzah, M.R. Mak'ruf, Peak flow meter with measurement analysis, Indonesian J. Electron. Electromed. Eng. Med. Inf. 2 (3) (2020) 107–112.
[10] C. Qiu, F. Wu, W. Han, M.R. Yuce, A wearable bioimpedance chest patch for real-time ambulatory respiratory monitoring, IEEE Trans. Biomed. Eng. 69 (9) (2022) 2970–2981.
[11] A. Haleem, M. Javaid, R.P. Singh, R. Suman, Applications of Artificial Intelligence (AI) for cardiology during COVID-19 pandemic, Sustain. Oper. Comput. 2 (2021) 71–78.
[12] T. Shaik, X. Tao, N. Higgins, L. Li, R. Gururajan, X. Zhou, U.R. Acharya, Remote patient monitoring using artificial intelligence: Current state, applications, and challenges, Wiley Interdiscip. Rev. Data Min. Knowl. Discov. (2023) e1485.
[13] A.K. Kumar, M. Ritam, L. Han, S. Guo, R. Chandra, Deep learning for predicting respiratory rate from biosignals, Comput. Biol. Med. 144 (2022) 105338.
[14] M. Bahrami, M. Forouzanfar, Sleep apnea detection from single-lead ECG: A comprehensive analysis of machine learning and deep learning algorithms, IEEE Trans. Instrum. Meas. 71 (2022) 1–11.
[15] D.M. Molla, H. Badis, L. George, M. Berbineau, Software defined radio platforms for wireless technologies, IEEE Access 10 (2022) 26203–26229.
[16] Y. Ge, A. Taha, S.A. Shah, K. Dashtipour, S. Zhu, J. Cooper, Q.H. Abbasi, M.A. Imran, Contactless WiFi sensing and monitoring for future healthcare-emerging trends, challenges, and opportunities, IEEE Rev. Biomed. Eng. 16 (2022) 171–191.
[17] T. Bhowmik, R. Mojumder, D. Ghosh, I. Banerjee, An evaluative review on various tele-health systems proposed in COVID phase, in: International Conference on Computational Intelligence in Pattern Recognition, Springer, 2022, pp. 201–210.
[18] M.B. Khan, A. Mustafa, M. Rehman, N.A. AbuAli, C. Yuan, X. Yang, F.H. Shah, Q.H. Abbasi, Non-contact smart sensing of physical activities during quarantine period using SDR technology, Sensors 22 (4) (2022) 1348.
[19] M.A.M. Al-hababi, M.B. Khan, F. Al-Turjman, N. Zhao, X. Yang, Non-contact sensing testbed for post-surgery monitoring by exploiting artificial-intelligence, Appl. Sci. 10 (14) (2020) 4886.
[20] H. Chen, X. Yuan, Z. Pei, M. Li, J. Li, Triple-classification of respiratory sounds using optimized s-transform and deep residual networks, IEEE Access 7 (2019) 32845–32852.
[21] M. Rehman, R.A. Shah, M.B. Khan, N.A. AbuAli, S.A. Shah, X. Yang, A. Alomainy, M.A. Imran, Q.H. Abbasi, Rf sensing based breathing patterns detection leveraging usrp devices, Sensors 21 (11) (2021) 3855.
[22] C. Yuan, M.B. Khan, X. Yang, F.H. Shah, Q.H. Abbasi, Cheyne-Stokes respiration perception via machine learning algorithms, Electronics 11 (6) (2022) 958.
[23] M. Rehman, N.A.A. Ali, R.A. Shah, M.B. Khan, S.A. Shah, A. Alomainy, X. Yang, M.A. Imran, Q.H. Abbasi, Development of an intelligent real-time multiperson respiratory illnesses sensing system using SDR technology, IEEE Sens. J. 22 (19) (2022) 18858–18869.
[24] R.X.A. Pramono, S. Bowyer, E. Rodriguez-Villegas, Automatic adventitious respiratory sound analysis: A systematic review, PLoS One 12 (5) (2017) e0177926.
[25] E. Hosseini-Asl, G. Gimel'farb, A. El-Baz, Alzheimer's disease diagnostics by a deeply supervised adaptable 3D convolutional network, 2016, arXiv preprint arXiv:1607.00556.
[26] M.J. Van Grinsven, B. van Ginneken, C.B. Hoyng, T. Theelen, C.I. Sánchez, Fast convolutional neural network training using selective data sampling: Application to hemorrhage detection in color fundus images, IEEE Trans. Med. Imaging 35 (5) (2016) 1273–1284.
[27] Y. Song, L. Zhang, S. Chen, D. Ni, B. Lei, T. Wang, Accurate segmentation of cervical cytoplasm and nuclei based on multiscale convolutional network and graph partitioning, IEEE Trans. Biomed. Eng. 62 (10) (2015) 2421–2433.
[28] O. Oktay, W. Bai, M. Lee, R. Guerrero, K. Kamnitsas, J. Caballero, A. de Marvao, S. Cook, D. O'Regan, D. Rueckert, Multi-input cardiac image super-resolution using convolutional neural networks, in: Medical Image Computing and Computer-Assisted Intervention-MICCAI 2016: 19th International Conference, Athens, Greece, October 17-21, 2016, Proceedings, Part III, Vol. 19, Springer, 2016, pp. 246–254.
[29] P. Kisilev, E. Sason, E. Barkan, S. Hashoul, Medical image description using multi-task-loss CNN, in: Deep Learning and Data Labeling for Medical Applications: First International Workshop, LABELS 2016, and Second International Workshop, DLMIA 2016, Held in Conjunction with MICCAI 2016, Athens, Greece, October 21, 2016, Proceedings. Vol. 1, Springer, 2016, pp. 121–129.
[30] Y. Bengio, P. Simard, P. Frasconi, Learning long-term dependencies with gradient descent is difficult, IEEE Trans. Neural Netw. 5 (2) (1994) 157–166.
[31] H. Salehinejad, S. Sankar, J. Barfett, E. Colak, S. Valaee, Recent advances in recurrent neural networks, 2017, arXiv preprint arXiv:1801.01078.
[32] F. Ullah, M. Bilal, S.-K. Yoon, Intelligent time-series forecasting framework for non-linear dynamic workload and resource prediction in cloud, Comput. Netw. 225 (2023) 109653.
[33] A. Ullah, J. Ahmad, K. Muhammad, M. Sajjad, S.W. Baik, Action recognition in video sequences using deep bi-directional LSTM with CNN features, IEEE Access 6 (2017) 1155–1166.
[34] J. Amoh, K. Odame, Deep neural networks for identifying cough sounds, IEEE Trans. Biomed. Circuits Syst. 10 (5) (2016) 1003–1011.
[35] H. Nakano, T. Furukawa, T. Tanigawa, Tracheal sound analysis using a deep neural network to detect sleep apnea, J. Clin. Sleep Med. 15 (8) (2019) 1125–1133.
[36] H. Ryu, J. Park, H. Shin, Classification of heart sound recordings using convolution neural network, in: 2016 Computing in Cardiology Conference, CinC, IEEE, 2016, pp. 1153–1156.
[37] J. Drzazga, B. Cyganek, An LSTM network for apnea and hypopnea episodes detection in respiratory signals, Sensors 21 (17) (2021) 5858.
[38] S. Li, Z. Li, J. Zhang, H. Zhang, A denoising method of diaphragm electromyogram signals based on dual-threshold filter, J. Mech. Med. Biol. 22 (03) (2022) 2240009.
[39] H.Y. Mir, O. Singh, Adaptive data analysis methods for biomedical signal processing applications, in: AI-Enabled Smart Healthcare using Biomedical Signals, IGI Global, 2022, pp. 52–71.
[40] E. Bas, E. Egrioglu, E. Kolemen, Training simple recurrent deep artificial neural network for forecasting using particle swarm optimization, Granular Comput. 7 (2) (2022) 411–420.
[41] L. Wang, J.P. Near, N. Somani, P. Gao, A. Low, D. Dao, D. Song, Data capsule: A new paradigm for automatic compliance with data privacy regulations, in: Heterogeneous Data Management, Polystores, and Analytics for Healthcare: VLDB 2019 Workshops, Poly and DMAH, Los Angeles, CA, USA, August 30, 2019, Revised Selected Papers, Vol. 5, Springer, 2019, pp. 3–23.